ANNALS of Clinical and Translational Neurology
Open Access
AMERICAN NEUROLOGICAL ASSOCIATION

RESEARCH ARTICLE

Downregulation of SF3B2 protects CNS neurons in models of multiple sclerosis

Ye Eun Jeong[1,3], Labchan Rajbhandari[1], Byung Woo Kim[2,4], Arun Venkatesan[1] & Ahmet Hoke[1]

[1]Department of Neurology, Johns Hopkins University School of Medicine, Baltimore, Maryland, 21205, USA
[2]Division of Neuropathology, Department of Pathology, Johns Hopkins University School of Medicine, Baltimore, Maryland, 21205, USA

Correspondence
Ahmet Hoke, Department of Neurology, Johns Hopkins University School of Medicine, Baltimore, MA 21205, USA. Tel: 410-955-2227; Fax: 410-502-5459; E-mail: ahoke@jhmi.edu

Present address
[3]Division of Applied Regulatory Science, Center for Drug Evaluation and Research, Food and Drug Administration, Silver Spring, Maryland, USA
[4]Division of Cellular and Gene Therapies, Office of Tissue and Advanced Therapies, Center for Biologics Evaluation and Research, Food and Drug Administration, Silver Spring, Maryland, USA

Funding Information
No funding information provided.

Received: 3 October 2022; Revised: 21 November 2022; Accepted: 21 November 2022

Annals of Clinical and Translational Neurology **2023; 10(2): 246–265**

doi: 10.1002/acn3.51717

[Correction added on 19 January 2023, after first online publication: The affiliation and present address for Byung Woo Kim was corrected.]

Abstract

Objective: Neurodegeneration induced by inflammatory stress in multiple sclerosis (MS) leads to long-term neurological disabilities that are not amenable to current immunomodulatory therapies. **Methods and Results**: Here, we report that neuronal downregulation of Splicing factor 3b subunit 2 (SF3B2), a component of U2 small nuclear ribonucleoprotein (snRNP), preserves retinal ganglion cell (RGC) survival and axonal integrity in experimental autoimmune encephalomyelitis (EAE)-induced mice. By employing an in vitro system recapitulating the inflammatory environment of MS lesion, we show that when SF3B2 levels are downregulated, cell viability and axon integrity are preserved in cortical neurons against inflammatory toxicity. Notably, knockdown of SF3B2 suppresses the expression of injury-response and necroptosis genes and prevents activation of Sterile Alpha and TIR Motif Containing 1 (Sarm1), a key enzyme that mediates programmed axon degeneration. **Interpretation**: Together, these findings suggest that the downregulation of SF3B2 is a novel potential therapeutic target to prevent secondary neurodegeneration in MS.

Introduction

MS is a chronic autoimmune inflammatory disease of the central nervous system (CNS), characterized by demyelination of axons, and secondary neurodegeneration. It is a disabling neurological disease affecting primarily young female adults and causes numbness or weakness in limbs, optic neuritis, gait ataxia, pain and fatigue, or sphincter dysfunction.[1,2] Current therapies primarily focus on modulating the autoimmune response, and are quite effective in alleviating the inflammation, but clinical need to develop neuroprotectant strategies to prevent irreversible neuro-axonal injury persists.[3,4]

Splicing Factor 3B Subunit 2 (SF3B2) is part of the SF3B complex which is an essential component of the spliceosome and is required for accurately recognizing the branch point of pre-messenger RNAs during splicing process.[5,6] Previously, we had shown that SF3B2 may have an additional neuroprotective function in the peripheral nervous system,[7] aside from its canonical role as a splicing

factor.[5,6] Reducing SF3B2 protein by RNAi in rat sensory neurons was sufficient to prevent cisplatin-induced neurotoxicity in vitro.[7] However, the effect of SF3B2 knockdown in CNS neurons and its underlying mechanism have not been studied yet.

Here, we report that reducing SF3B2 expression by multiple gene silencing techniques makes cortical neurons resistant to subsequent degeneration triggered by neurotoxic inflammatory stress. Specifically, AAV-mediated knockdown of SF3B2 substantially prevents RGC loss, and demyelination and axon degeneration in optic nerves of EAE mice compared to the EAE group treated with control AAV. We further confirmed the neuroprotective effect of lowering SF3B2 levels in cortical neurons cultured in a microfluidic platform mimicking inflammatory active lesions of MS and found that RNAi-mediated knockdown of SF3B2 preserved axonal integrity when challenged with neurotoxic microglia media conditioned by lipopolysaccharide (LPS). This was associated with suppression of mRNA levels of regeneration-associated genes and necroptosis genes, and prevention of activation of Sarm1, a key enzyme mediating programmed axon degeneration. These findings suggest that targeting SF3B2 could serve as an effective therapeutic strategy to prevent neurodegeneration in inflammatory CNS diseases.

Materials and Methods

Mice

C57BL/6J female mice at the age of 7 weeks were purchased from Jackson Laboratory. Before the intravitreal injection and EAE induction procedure, mice were anesthetized by i.p. injection of ketamine (120 mg/kg) and xylazine (8 mg/kg). All animal experiments were conducted following the protocols approved by Institutional Animal Care and Use Committee at Johns Hopkins University School of Medicine.

EAE induction and clinical scoring

Two weeks post-AAV vector delivery, EAE was induced in C57BL/6J female mice as previously described.[8] Emulsion containing 150 μg of MOG_{33-55} (AnaSpec) in complete Freund's adjuvant (CFA) (MilliporeSigma) with 600 μg of *Mycobacterium tuberculosis* (BD) was subcutaneously injected into both sides of the lateral abdomen. A 375 ng of pertussis toxin (List Biologicals) was injected intraperitoneally on days 0 and 2. For healthy controls, the same emulsion without MOG_{33-55} peptide was used. EAE clinical symptoms were monitored on a daily basis following Hooke lab's Mouse EAE scoring guidelines.

Design and production of AAV vectors expressing shRNAs

Two shRNA sequences targeting SF3B2 were selected using the TRC shRNA design process offered by Broad Institute (https://portals.broadinstitute.org/gpp/public/resources/rules). H1 promoter and two shRNAs were synthesized and cloned into HindIII and BamHI sites of pAAV-U6-CMV-GFP vector provided by the Boston Children's Hospital Viral Core. shRNA synthesis and subcloning were done by GenScript, and all plasmids were packaged into AAVs by the same Viral Core. The AAV titers used for this study were in the range of 1.48–8.02 × 10^{12} genome copy (GC)/ml. (Two targeting sequences against SF3B2: 5′-CCGG-GCTCGTCACTTCCTGTTCTTA-CTCGAG-TAAGAACAG GAAGTGACGAGC-TTTTTG-3′, and 5′-CCGG-CTGATT GCCATGCAGCGATAT-CTCGAG-ATATCGCTGCATGG CAATCAG-TTTTTG-3′, scrambled shRNA sequence: 5′-CTAAGGTTAAGTCGCCCTCG-CTCGAG-CGAGGGC GACTTAACCTTAGG-3′)

Intravitreal injection of AAV vectors

At 8–9 weeks of age, 1.2 μl of AAV with a titer of 1.5 × 10^{12} gc/ml in PBS was delivered into the mouse vitreous. After anesthetizing mice with Ketamine/Xylazine, a small hole was made ~1 mm posterior to the limbus. Injection was carefully performed with a 32-gauge microliter Hamilton syringe without damaging the lens.

Retina and optic nerve tissue preparation

Mice were sacrificed by a lethal dose of isoflurane and perfused with 50 ml ice-cold phosphate-buffered saline (PBS). Eyes were removed and fixated in 4% paraformaldehyde for 1 h at room temperature and kept in ice-cold PBS until immunofluorescence staining. Optic nerves were removed and post-fixed in ice-cold 3% glutaraldehyde/4% paraformaldehyde in 0.1 M Sorensen's phosphate buffer for 72 h at 4°C, and washed with ice-cold 0.1 M Sorensen's phosphate buffer for 48 h at 4°C.

Whole mount retina staining and RGC density analysis

Retinas were isolated from the eyes and blocked with 10% normal goat serum/1% Triton-X 100 in PBS (1% PBST) at room temperature for 30 min, and incubated with primary antibodies in 1% PBST for 48 h at 4°C. Following is the antibody information: Mouse anti-BRN3A (Cat: MAB1585, MilliporeSigma, 1:250); Rabbit anti-SF3B2 (Cat: A301-605A, Bethyl, 1:300). Whole retinas were washed with 1% PBST for 6–8 h at room

temperature and incubated with Alexa Fluor secondary antibodies in 1% PBST for 24 h at 4°C. Washed retinas were cut into four leaflets and flat-mounted onto slides. RGC counting was conducted as previously described[8] with some modifications. Specifically, retinal images were captured using Zeiss LSM 800 confocal microscope and Zen software with a z-stack interval of 3 μm with the same parameters and setting, and randomly selected 12 regions (central, medial, peripheral parts from the center of retina and four leaflets) were examined for counting RGCs. To assess the knockdown efficiency of AAV2/PHP.eb-SF3B2 shRNA in RGCs, images were taken with z-stack interval of 1/2 airy unit (0.45 μm) and the setting conditions were same across all samples. Since the promoter for GFP is different from the promoters directing shRNA expression, both regions having faint and strong GFP signals were included for this analysis. 3D images were constructed and SF3B2 fluorescence intensity per volume in BRN3A+ cells was semi-automatically measured by Imaris 9.5 software. The entire process of imaging and analysis was done in a blinded fashion.

Electron microscopy and axon quantification

Fixed optic nerves were transferred from Sorenson's buffer and post-fixed in 2% osmium tetroxide and later dehydrated in graded ethanol. The tissue was then embedded in Embed 812 (Electron Microscopy Sciences) and 1 micron sections were stained on slides with 1% toluidine blue. For electron microscopy, 70 nm sections were cut with a Reicher-Jung Ultracut E ultramicrotome and placed on 100 mesh formvar coated grids and viewed on a Zeiss Libra 120 at an accelerating voltage of 120 kV, using a Veleta camera (Olympus). To evaluate RGC axonal integrity, 10 randomly selected areas per each optic nerve sample were imaged, and the density of healthy myelinated axons and degenerating axons and g-ratio were manually quantified in a blinded manner.

Primary culture of mouse cortical neurons

C57BL/6J pregnant mice were purchased from Jackson Laboratory. Cortices were isolated from embryonic day (E) 16 mouse embryos. Dissected tissues were dissociated with 0.25% trypsin and cells were counted using a hemocytometer and 0.2% trypan blue to exclude dead cells. Cells were seeded in tissue culture (TC)-treated plates precoated with Matrigel and microfluidic devices precoated with poly-D-lysine. Cortical neurons were cultured in Neurobasal medium containing 2% B-27 supplement, 1% N-2 supplement, 0.5% GlutaMAX, 0.5% non-essential amino acids (NEAA), and 1% penicillin/streptomycin for the first 3 days. Half of the medium was changed with fresh Neurobasal medium supplemented with 2% B-27 supplement, 1% N-2 supplement, and 1% penicillin/streptomycin every 2–3 days.

Neuro-2a (N2a) cell culture

N2a cells (CLL-131) were purchased from American Type Culture Collection (ATCC). Cells with passage number 7–8 were used for experiments. Cells were maintained in Dulbecco's modified eagle medium (DMEM) supplemented with 10% heat-inactivated fetal bovine serum (FBS) and 1% penicillin/streptomycin. N2a cells were differentiated using DMEM with 1% FBS and 10uM retinoic acid (RA) (Sigma, R2625) for 2 days following transfection with siRNA.

Conditioned medium from LPS-stimulated microglia cell line (MCM)

SIM-A9 cells (CRL-3265) were obtained from ATCC. Cells with passage number 8–9 were used for experiments. Cells were cultured in DMEM/F12 medium plus 10% FBS, 1% penicillin/streptomycin. To prepare conditioned medium for further experiments, SIM-A9 cells were stimulated in DMEM/F12 medium containing 1% FBS and 100 ng/ml LPS or 2% FBS and 2000 ng/ml LPS (Sigma, L6529), for N2A cells or cortical neurons, respectively. Twenty-four hours later, supernatant was collected and used for experiments. Freshly prepared conditioned medium was used for all experiments.

Transfection and plasmid

Primary mouse cortical neurons (DIV2) or N2A cells were transfected with siRNA using Lipofectamine RNAiMAX (Thermo Fisher Scientific, 13778100) and plasmid DNA using Lipofectamine 3000 (Thermo Fisher Scientific, L3000001) following the manufacturer's protocol with a minor modification. Cells were incubated with serum-free medium for 1–2 h prior to transfection and replenished with fresh complete medium 5–6 h post-transfection. Six nanometers of siRNA for N2A cells and 25 nM of siRNA for cortical neurons were used, and 2.0 μg and 0.5 μg of DNA plasmid were added onto N2A cells cultured in 6-well plates and 24-well plates, respectively. siRNAs were purchased from Ambion (SF3B2 siRNA: S147808, negative control siRNA: 4390846). pcDNA3.1(+)-SF3B2-GFP contains the coding sequence of the mouse SF3B2 gene (NM_030109.2) under the control of CMV promoter, and the control backbone vector expressing GFP was used as a control. Plasmids were purchased from GenScript.

Cortical neuronal culture on microfluidic devices

5×10^4 cortical neurons were seeded onto the cell body sector of devices precoated with poly-D-lysine (PDL) at 100 μg/ml. At day 6, lentiviral particles at MOI 140 were added into the cell body sector, and 72 h later, axons growing in the axonal compartment were challenged with MCM for 24 h.

ATP measurements

Intracellular levels of ATP were measured using ViaLight Plus BioAssay kit (Lonza, LT07-121, 221). 5×10^4 cortical neurons or 7×10^3 N2a cells were seeded on Matrigel-precoated 96-well plate, and transfection with siRNA was performed at 2 days in vitro (DIV) for cortical neurons and at day 1 for N2a cells. Cortical neurons were incubated with 1:1 mixture of microglial conditioned media (MCM) with LPS and neurobasal medium containing 2% B27 minus AO (Thermo Fisher Scientific, 10889038). For N2a cells, 1:1 mixture of MCM with LPS and DMEM containing 1% FBS and 10uM retinoic acid was added. After 48 h, ATP levels in each well were measured using *LMax* II luminescence microplate reader. MCM without LPS incubation was used as a control.

Caspase activity assays

Caspase-Glo® 3/7 and 8 assays (Promega G8091, G8201) were used to assess the activity of caspase-3/7 and -8 in neurons. 2×10^3 N2a cells were seeded on Matrigel-coated 96-well plate 24 h before the transfection and 1:1 mixture of MCM with LPS and DMEM containing 1% FBS and 10 μM retinoic acid was added. The activity of caspases was measured using *LMax* II luminescence microplate reader. MCM without LPS incubation was used as a control.

NAD+ measurements

Concentrations of NAD+ were measured using NAD+/NAD+H-Glo Assay kit (Promega G9071, 9072). 2×10^4 cortical neurons or 2×10^3 N2a cells were seeded in Matrigel-precoated 96 well plate. For cortical neurons, cells were transfection with siRNA at DIV 2 and incubated with 1:1 mixture of microglial conditioned media (MCM) with LPS and neurobasal medium containing 2% B27 minus AO (Thermo Fisher Scientific, 10889038) for 24 h. N2A cells were transfected with 0.125 μg of plasmid DNA and NAD+ concentrations were measured using *LMax* II luminescence microplate reader following the manufacturer's protocol. MCM without LPS incubation was used as a control.

Drug treatments

All compounds were dissolved in DMSO (D2650, MilliporeSigma) and diluted with cell culture media. For apoptosis inhibitors, a pan-caspase inhibitor z-VAD-FMK (FMK001, R&D systems) was used at 50 μM, z-DEVD (FMK004, R&D systems), targeting Caspase-3, -6, -7, -8, and -10, was used at 25 μM, Wedelolactone (401474, Calbiochem), targeting Caspase-11, was used at 10 μM, z-WEHD-FMK (FMK002, R&D systems), targeting Caspase-1, -8, and -11, was used at 20 μM, VX-765 (S2228, Selleckchem), targeting Caspase-1 and -4, was used at 20 μM, z-YVAD-FMK (218746, MilliporeSigma), targeting Caspase-1 and -11, was used at 20 μM, z-VEID-FMK (FMK006, R&D systems), targeting Caspase-6, was used at 10 μM. For necroptosis inhibitors, Necrostatin-1 (N9037, MilliporeSigma), targeting RIPK1, was used at 50 μM, and GSK872' (6492, R&D systems), targeting RIPK3, was used at 2 μM. Both inhibitors and vehicle (DMSO) were added to the cell culture medium 1–2 h prior to the treatment of MCM and control media.

Western blotting

Protein lysates were prepared using radioimmunoprecipitation assay (RIPA) buffer (Thermo Fisher Scientific, 89901), and concentrations were determined by BCA assay (Thermo Fisher Scientific, 23225). Ten micrograms of proteins were loaded and run on mini-protean TGX precast protein gels (Biorad, 456-1094, 145-1106) and transferred onto trans-blot turbo midi 0.2 μm polyvinylidene difluoride (PVDF) membranes (Biorad, 170-4157). The membranes were blocked with 5% blotting-grade blocker in tris-buffered saline with 0.1% tween 20 detergent (TBST) for 30 min and incubated with primary antibodies diluted in blocking buffer for overnight at 4°C. Following is the antibody information: Rabbit anti-SF3B2 (Cat: A301-605A, Bethyl, 1:2000); Rabbit anti-SF3B3 (Cat: A302-508A-T, Bethyl, 1:1000); Rabbit anti-SF3B4 (Cat: A303-950A-T, Bethyl, 1:1000); Rabbit anti-Caspase-3 (Cat: 9662, Cell signaling technology (CST), 1:1000); Rabbit anti-Cleaved caspase-3 (Cat: 9661, CST, 1:1000); Mouse anti-β-actin (Cat: AC004, Neo Scientific, 1:4000). After triple washing steps, membranes were probed with secondary antibodies conjugated with HRP (goat anti-rabbit IgG antibody), HRP-conjugate (MilliporeSigma, 12-348, 1:2000), and goat anti-mouse IgG H&L HRP (Abcam, ab6789, 1:2000) for 1 h at RT. Bands were detected with Pierce ECL western blotting substrate (Thermo Fisher Scientific, 32106).

Lentivirus generation

The third-generation pLL3.7 (plasmid #11795) lentiviral vector was purchased from Addgene, and U6 promoter with SF3B2

shRNAs or scrambled shRNA were cloned into *Not*I and *Nsi*I sites of a backbone plasmid. All plasmids were packaged into lentivirus by the Boston Children's Hospital Viral Core. Two shRNA sequences targeting mouse SF3B2 are listed in Table 1, and scrambled shRNA sequence is 5′-CCTAAGGTT AAGTCGCCCTCG-CTCGAG-CGAGGGCGACTTAACCTTA GG-3′.

Immunofluorescence staining

Cells were fixed in 4% paraformaldehyde for 50 min at room temperature and washed three times with PBS. Fixed cells were permeabilized and blocked with 0.25% Triton X-100 and 5% goat serum in PBS for 30 min. Cells were incubated with mouse monoclonal anti-TAU-1 (1:300, MilliporeSigma, MAB3420) diluted in blocking solution overnight at 4°C. Non-immune IgG isotype (Thermo Fisher Scientific, 10400C) was used as a negative control at concentration identical to the primary antibody. Following primary antibody incubation, cells were rinsed in PBS twice and incubated with Alexa Fluor 555 anti-mouse secondary antibody (1:500, Thermo Fisher Scientific, A21424) diluted in blocking solution for 2 h at RT. Cells were washed in PBS, stained with Hoechst 33342 (1:5000, Thermo Fisher Scientific, 62249) for nuclear visualization, and then rinsed in PBS three times for visualization.

Axon outgrowth analysis

Primary cortical neurons in microfluidic chambers were infected with lentiviral shRNA (MOI of 140) for 24 h at day 6, and treated with microglial CM at day 9 for 24 h. To evaluate axon sprouting, areas covered by Tau-1 positive axons and the number of axons extending beyond 750um from the opening of the channels were quantified.

Knockdown efficiency of lentiviral SF3B2 shRNAs by RT-PCR

Primary cortical neurons were infected with lentivirus at MOI of 140 for 3 days. Total RNA was purified using Trizol (Thermo Fisher Scientific, 15596026) and RNA isolation kit (Zymo Research, R2070) following manufacturers' protocol. Reverse transcription was carried out using SuperScript VILO cDNA Synthesis Kit (Thermo Fisher Scientific, 11754050), and 500 ng of cDNA samples in duplicate were analyzed in LightCycler 480 Real-Time PCR system (Roche) with KiCqStart SYBR GREEN qPCR ReadyMix (Sigma, KCQS00). RNA and DNA concentrations were determined by Nano Drop 2000 (Thermo Fisher Scientific). RT-PCR data were normalized to the mean of three housekeeping genes mRNA expression levels (HPRT1, HMBS, 18 S rRNA).

Table 1. Short hairpin sequences targeting mouse SF3B2.

#1	5′-CCGG-GCTCGTCACTTCCTGTTCTTA-CTCGAG-TAAGAACAGGAAGTGACGAGC-TTTTTG-3′
#2	5′-CCGG-CTGATTGCCATGCAGCGATAT-CTCGAG-ATATCGCTGCATGGCAATCAG-TTTTTG-3′

RNA isolation and quantitative PCR

Total RNAs of cortical neurons were extracted at 24 h post-MCM incubation. Detailed experimental steps were described above. KiCqStart SYBR Green Primers were purchased from MilliporeSigma. Primer sequences for all 25 genes of interest are listed in Table S1.

Statistical analysis

All statistical analyses were performed by *t*-test, two-way ANOVA, simple linear regression or one-way ANOVA with Tukey's multiple comparison test using GraphPad (Prism version 9). All data are presented as mean ± SEM. Statistical significance was considered when *p*-value was less than 0.05.

Results

AAV-mediated knockdown of SF3B2 improves the survival of RGCs in EAE mice

To determine whether reduction of SF3B2 prevents RGCs from inflammation-induced degeneration,[9] we employed AAV2/PHP.eb particles possessing a tropism toward CNS neurons[10,11] in EAE mice. We introduced the virus intravitreally and first confirmed the knockdown efficiency and safety of AAV vectors expressing *Sf3b2* shRNA (Figs. S1 and S2). For the analysis of RGC survival, we included EAE mice whose clinical scores peaked at 3.0 and maintained mean clinical scores of at least 2.5. There was no difference in disease scores between EAE groups except on days 13 and 17, where the two EAE groups with virus injection had slightly higher clinical scores than uninjected EAE groups, which may be due to the additional experimental procedure for virus administration (Fig. 1A,B). In order to quantify the density of RGCs, we made four radial cuts in retinas and immunostained with brain-specific homeobox protein 3A (BRN3A), a pan-RGC marker.[12] Within each flattened retina, we separated central, medial, and peripheral regions from the center, and examined a total 12 areas in each retina (Fig. 1C). We confirmed that there was a dramatic loss of RGCs in both EAE-induced mice without virus injection and with AAV-GFP control virus injection compared to healthy Complete Freund's adjuvant (CFA)-

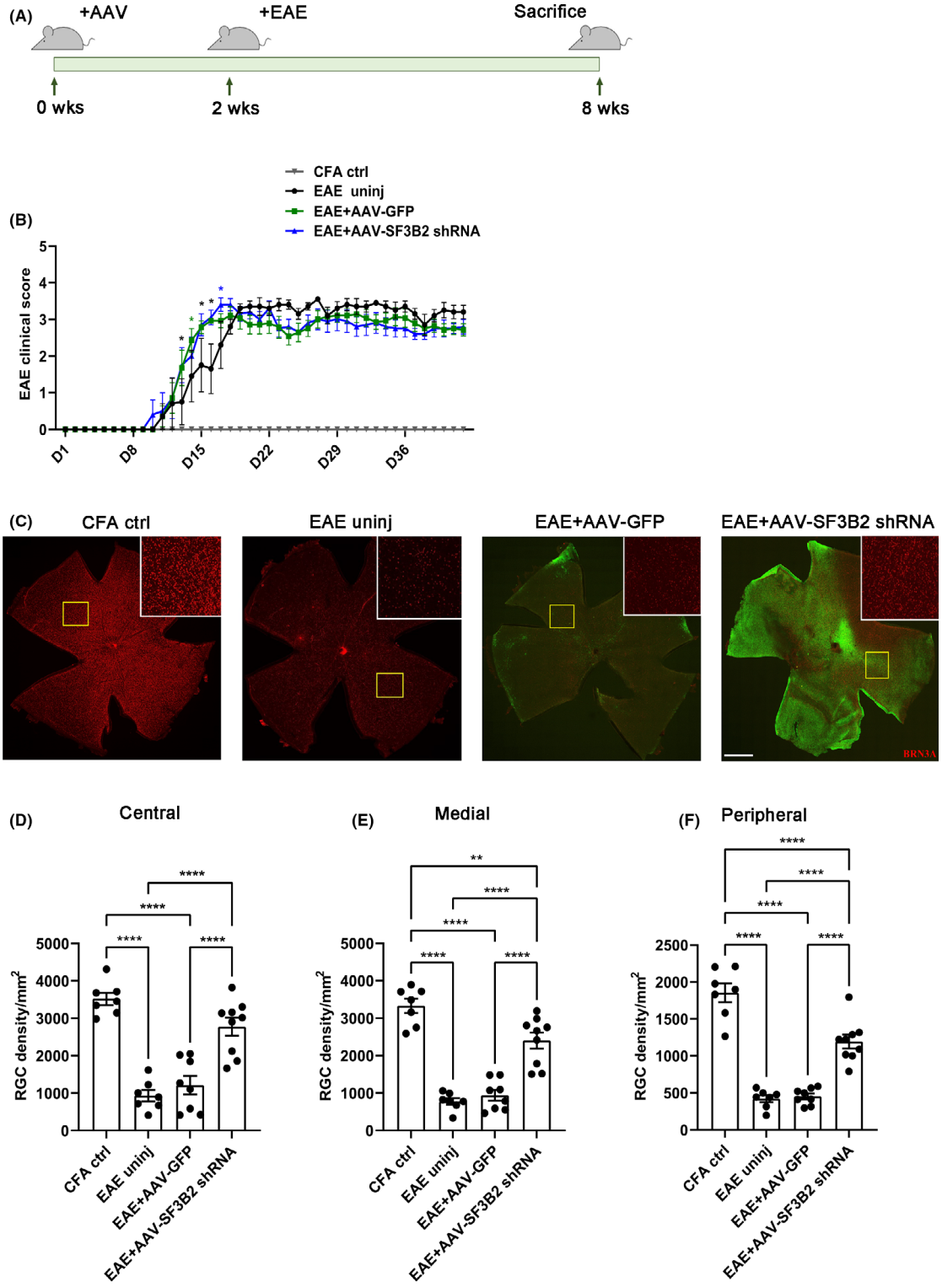

Figure 1. AAV-mediated knockdown of SF3B2 prevents RGC death in EAE mice. (A) Timeline of AAV administration and EAE experiment. (B) Clinical scores of CFA control and EAE-induced mice ($n \geq 5$). (C) Representative images of whole-mount retinas immunostained with Brn3a. Scale bar = 500 μm. (D–F) Quantifications of densities of Brn3a + RGCs in the central (D), medial (E), and peripheral regions (F) of retina (total number of samples is seven for CFA control and EAE uninj, eight for EAE + AAV-GFP, nine for EAE + AAV-*Sf3b2* shRNA). All data are shown as mean ± SEM of combined data from three independent experiments. *$p < 0.05$, **$p < 0.01$, ***$p < 0.001$, ****$p < 0.0001$.

injected control mice. In contrast, reducing SF3B2 levels by AAV-*Sf3b2* shRNA prevented the loss of RGCs from retrograde degeneration caused by axon injury. We found that RGC densities were significantly higher in all three regions of retinas from EAE mice administered AAV-SF3B2 shRNA compared to both EAE mice injected with AAV-GFP and EAE mice without virus injection (EAE wo inj) (Fig. 1D–F). These results suggest that downregulating the cellular level of SF3B2 makes RGCs resistant to inflammatory neurodegeneration.

Downregulated SF3B2 preserves axonal integrity and myelination in EAE mice

To further verify whether the reduction of SF3B2 by virus delivery also protects the integrity of RGC axons and their myelination, we examined optic nerve sections by transmission electron microscopy (TEM) (Fig. 2A). We counted 10 randomly selected areas per each optic nerve and quantified the number of myelinated axons having discernible neurofilaments and tightly formed myelin sheaths (Fig. 2B). We also counted the degenerating axons with distinct patterns of Wallerian-like degeneration and disrupted filaments[13] (Fig. 2C,D). We found that there were higher densities of myelinated axons in EAE mice administered AAV-*Sf3b2* shRNA compared to both EAE wo inj and EAE with AAV-GFP, demonstrating that myelinated axons were preserved in EAE mice with SF3B2 reduction (Fig. 2B). There were fewer degenerating and unmyelinated axons when compared to both EAE wo inj and EAE with AAV-GFP groups (Fig. 2C,D). Together, these results indicate that demyelination and axonal degeneration that occurred during EAE progression were substantially suppressed in EAE with SF3B2 downregulation.

In addition, we also examined the size of axons and thickness of myelin sheaths. As shown in Fig. 2E, g-ratio in EAE with reduced SF3B2 tended to be lower than the other two EAE disease controls, indicating thicker myelin. However, there was no significant difference in average diameter of axon fibers among all groups (Fig. 2F). We then analyzed the distribution of myelinated nerve fibers using a scatter plot showing g-ratio as a function of inner axon diameter (Fig. 2G). All groups had similar g-ratios of smaller axons but in both groups of EAE mice without SF3B2 downregulation, g-ratios were higher in larger axons compared to CFA control and EAE with AAV-*Sf3b2* shRNA groups, indicating that larger axons were thinly myelinated during EAE progression when SF3B2 levels were not manipulated. Together, these results demonstrate that downregulation of SF3B2 preserves RGC axonal integrity and myelination against inflammatory injury induced in EAE mice.

Reduction of SF3B2 by RNAi protects axonal integrity and survival of cortical neurons challenged with LPS-stimulated microglia cell line media

To further dissect the mechanism of neuroprotection afforded by reduced SF3B2 levels, we examined the effects of reduced SF3B2 on axonal outgrowth and cell survival in an in vitro model of inflammatory neuronal injury. We first confirmed the antibody specificity and the ability of siRNA constructs to downregulate SF3B2 levels in vitro (Fig. S3). Using a microfluidic platform, a well-established system for evaluating axonal elongation,[14] we transduced cultured embryonic mouse primary cortical neurons (PCNs) with lentivirus expressing *Sf3b2* shRNA then exposed to the microglia cell line conditioned media (MCM), which is the supernatant of SIM-A9 microglia cell line stimulated with lipopolysaccharide (LPS). LPS is an endotoxin and a component of outer membrane of gram-negative bacteria.[15] When microglia are exposed to LPS, they release pro-inflammatory cytokines, such as interferon- γ (IFN-γ), tumor necrosis factor-α (TNF-α), and interleukin-6 (IL-6), which are important mediators of MS pathogenesis.[16–18] SIM-A9 microglia cell line was stimulated with LPS to mimic activated microglia.[19,20] First, we confirmed the neurotoxicity of MCM on Neuro-2A cells (N2A) as demonstrated by increase in cleaved caspase-3 and reduction in ATP levels (Fig. S4). In order to assess axonal degeneration induced by MCM directly, we immunostained PCN cultures in microfluidic chambers for axonal protein, Tau-1[21] and imaged the entire axonal compartment (Fig. 3A). To determine axonal projections, we semi-automatically analyzed areas covered by axons, and counted the number of axons extending beyond 750 μm from the opening of the channels. As seen in Fig. 3B,C, MCM caused degeneration of axons. In contrast, axons were protected from degeneration when SF3B2 was reduced, as indicated by substantially higher numbers of axons reaching over a set distance (3/4 of the entire axonal sector) as well as increased areas occupied by axonal processes (Fig. 3B,C). Consistent with this morphological observation, further biochemical analysis revealed that reduced SF3B2 expression prevented a decline in ATP levels as a measure of overall cellular toxicity.[22] Perhaps more importantly, it also prevented a decline in nicotinamide adenine dinucleotide (NAD+) concentrations which is degraded upon activation of Sarm1, a key enzyme in the programmed axon degeneration pathway[23,24] (Fig. 3E,F). Our findings substantiate the concept that reducing cellular level of SF3B2 not only supports neurons to maintain axonal outgrowth and integrity but also prevents cytotoxic effect triggered by inflammatory injury.

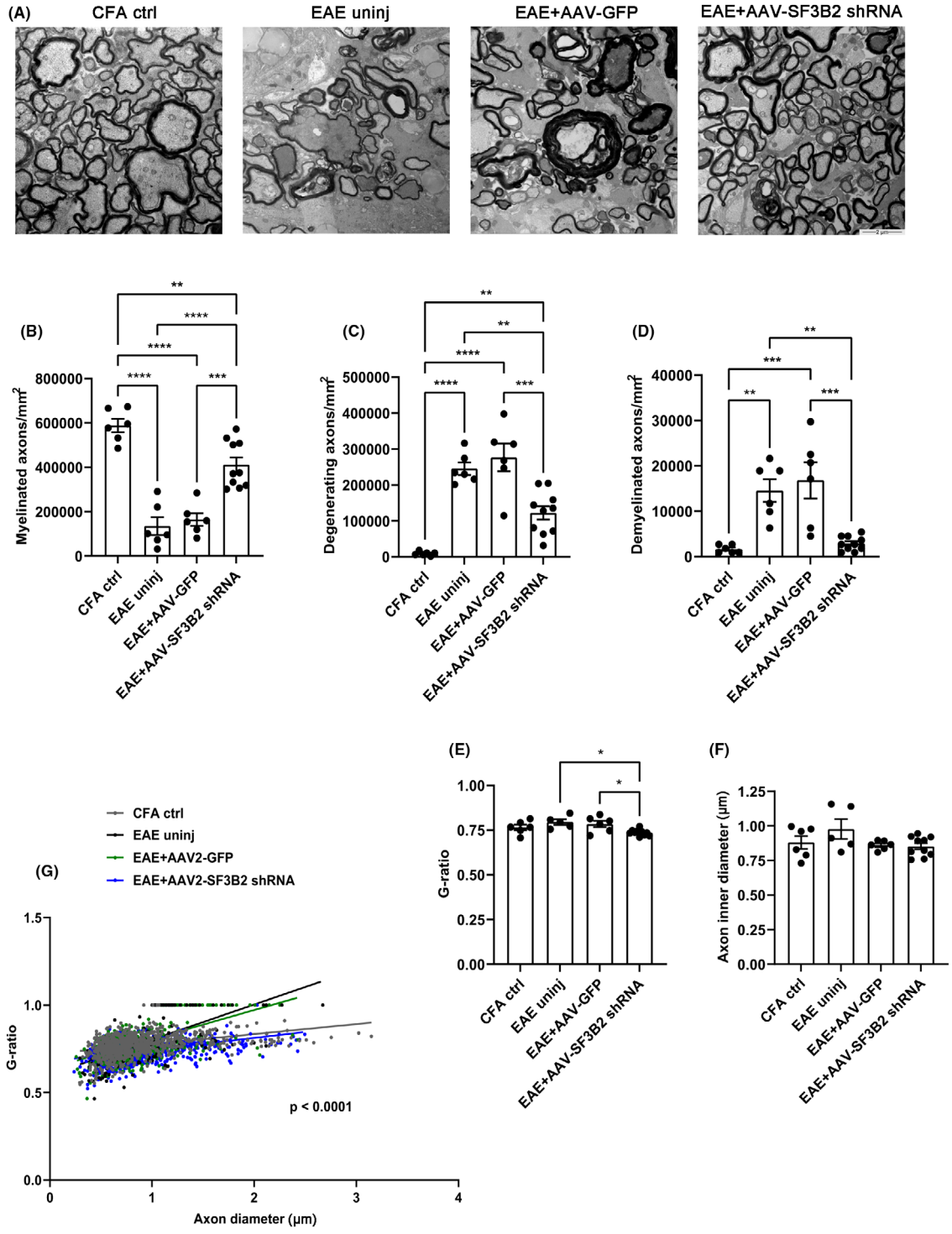

Figure 2. SF3B2 downregulation by AAV-shRNA attenuates axonal degeneration and demyelination in EAE mice. (A) Electron microscopy images of optic nerves. Scale bar = 2 μm. 10,000X mag. (B-D) Quantifications of densities of myelinated axons (B), degenerating axons (C), and demyelinated axons (D). For (D), demyelinated axons with a diameter larger than 1 μm were included (total number of samples is ≥6 for B–D). (E) Quantification of mean g-ratio of axons. (F) Quantification of mean axon diameter. (G) Scatter plot of g-ratio as a function of axon diameter for all groups. Linear regression analysis indicated a significant difference in slope between EAE mice treated with AAV-*Sf3b2* shRNA and the other two EAE-diseased groups (total number of samples is ≥5 for E–G and at least 160 axons per each condition were analyzed). All data are shown as mean ± SEM combined data from three independent experiments. *$p < 0.05$, **$p < 0.01$, ***$p < 0.001$, ****$p < 0.0001$.

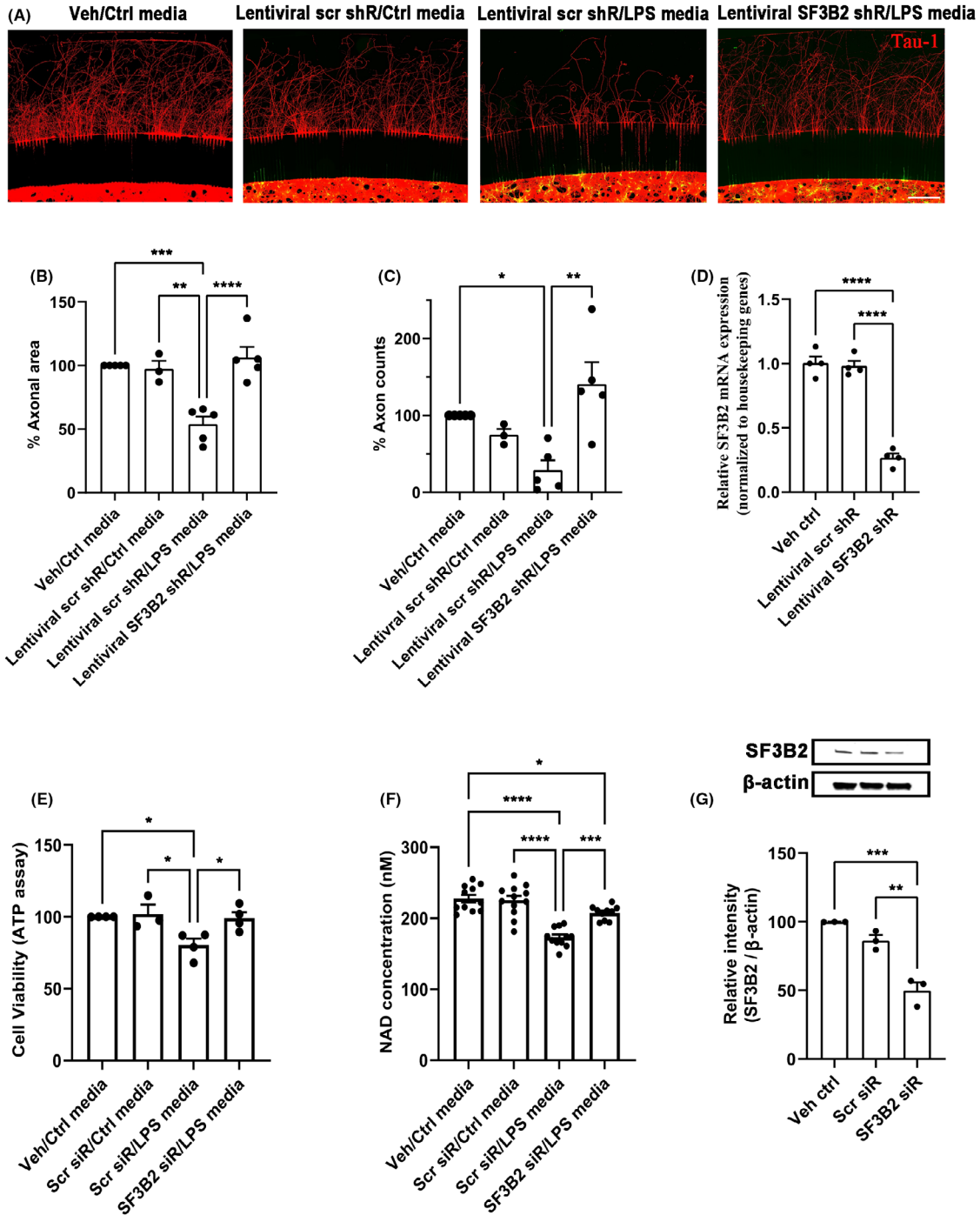

Figure 3. Lentiviral delivery of *Sf3b2* shRNA preserves axonal outgrowth and neuronal viability from MCM-induced toxicity. (A–C) Cortical neurons were challenged with MCM for 24 h at DIV9 following lentiviral transduction at DIV6. (A) Representative tiled images of cortical neurons cultured onto microfluidic devices. Neuronal cell bodies plated in the bottom compartment projected their Tau+ axons toward the upper axonal sector which is connected via 450 μm long microgrooves. (B) Percentage of areas covered by Tau-1 positive axons (n = 3–5). (C) Percentage of axons reaching over 750 μm from the entry of microgrooves (n = 3–5). (D) SF3B2 mRNA levels from cortical neurons transduced with lentivirus for 3 days (n = 4). (E, F) Cortical neurons were treated with MCM at DIV4 following siRNA transfection at DIV2. (E) Cell viability (n = 3–4) and (F) NAD+ concentrations of cortical neurons (n = 10–12). (G) Western blot analysis in cortical neurons transfected with scrambled siRNA or *Sf3b2* siRNA for 48 h (n = 4). Beta-actin was used as a loading control. All data are shown as mean ± SEM of three to five independent experiments. *p < 0.05, **p < 0.01, ***p < 0.001, ****p < 0.0001.

SF3B2 overexpression causes neurite degeneration

Given that knockdown of SF3B2 was neuroprotective against inflammatory injury to neurons, then we asked if overexpressing SF3B2 could exert any effect on neurite maintenance. To assess the impact of increased SF3B2 levels on neurite outgrowth and health, we examined the neurite morphology and measured NAD+ concentrations. N2A cells were transfected with a plasmid coding for GFP or SF3B2-GFP, and immunocytochemistry and NAD+ assay were carried out. In contrast to GFP control, N2A cells overexpressing SF3B2 had a threefold higher protein levels of SF3B2 and a marked reduction in the number of neurons with neurites, and those with neurites displayed fewer total number of branches and had shorter neurites (Fig. 4A–F). This pruning of neurite growth was correlated with significantly lowered NAD+ concentrations in cells with elevated level of SF3B2 compared to controls (Fig. 4G). These findings suggest that, in contrast to the protective effects of reduced SF3B2 on CNS neurons, SF3B2 overexpression is likely to impede neurite outgrowth and cause neurite degeneration.

Downregulation of SF3B2 in neurons prevents inflammatory damage

To identify which genes or pathways by which SF3B2 downregulation makes neurons resistant to degeneration, we investigated the expression levels of 25 candidate genes involved in injury-response, apoptosis, and necroptosis (please see Table S1 for full list). Primary mouse cortical neurons were allowed to establish in culture for 6 days, and infected with lentiviral shRNA for 72 h, and then challenged with MCM for 24 h prior to RNA isolation. After confirming downregulation of SF3B2 (Fig. 5A), we screened the mRNA levels of several regeneration-associated genes[25–29] (Fig. 5B). We found that inflammatory stress elicited by MCM markedly increased the transcription of several RAGs (*Atf3*, *Gadd45a*, *Gap43*, *Stmn2*, and *Tgfb1*), but not all, compared to the control groups. These genes have been shown to be upregulated upon neuronal damage,[25,26,28,29] thus, these observations confirm the neurotoxicity of MCM on cortical neurons. However, as shown in Fig. 5B, neurons with *Sf3b2* shRNA had substantially lowered transcriptional levels of four of these RAGs (*Atf3*, *Gap43*, *Myc*, and *Tgfb1*) similar to the controls, supporting the neuroprotective role of SF3B2 knockdown. Together, these findings indicate that SF3B2 downregulation enabled neurons to be resistant and less susceptible to inflammation-induced cellular damage.

Apoptosis is not the target mechanism by which SF3B2 reduction protects against MCM-induced inflammatory neurotoxicity

In addition to the analysis of regeneration-associated gene expression, we asked whether the transcriptional activation of caspase-dependent apoptosis genes and necroptosis could be modulated with a decline in SF3B2 level since these mechanisms have been shown to play a partial role in inflammation-induced neuronal death.[30–32] qPCR analysis of *Caspases-8*, *-9*, and *-3* involved in initiating and executing apoptotic death[33,34] showed that there was a small upregulation of *Caspase-8*, but not *Caspase-3* or *Caspase-9* with MCM and that there was no transcriptional difference between scrambled control and SF3B2 downregulated groups (Fig. 6). MCM treatment induced a small change in gene expression of *Bid* but no other members of the Bcl-2 family members. This small upregulation of *Bid* by MCM was not reversed by SF3B2 knockdown. Similarly, there were no significant differences in mRNA levels of *Calpain-1* and *Calpain-2* (Fig. 6). In addition to gene expression study, we examined whether SF3B2 downregulation influences the enzymatic activity of Caspase-3/7 and Caspase-8 in neuronal cells following MCM treatment. Although MCM-induced Caspase-3/7, but not Caspase-8 activity, this enzymatic activity induction was not blocked by downregulation of SF3B2 (Fig. 7A), suggesting that neuroprotective effect of knockdown of SF3B2 is not mediated through the regulation of apoptosis, but likely acting downstream from activation of Caspase-3. Contrary to what is seen with apoptosis gene expression, MCM-induced upregulation in the transcription of necroptosis-related genes, such as *Tnf-α*, *Ripk3*, and *Mlkl*,[30,35] was markedly attenuated in neurons where SF3B2 expression was knocked down with shRNA across multiple independent experiments (Fig. 8). Finally, we examined whether inhibitors targeting either caspases or necroptosis[36–39] could prevent MCM-induced axon degeneration and reduced NAD+ levels. Among the various caspase inhibitors, only z-VAD-FMK, the pan-caspase inhibitor,[39] prevented a reduction in NAD+ levels (Figs. 7B,C and S5). More selective inhibitors, such as z-DEVD-FMK, targeting Caspase-3, -7, -8, and -10,[40] and z-WEHD-FMK, targeting Caspase-1, -4, -5, and -8[41,42] and the specific Caspase-6 inhibitor z-VEID-FMK[43] did not block MCM-induced reduction in NAD+ levels. Wedelolactone, a selective inhibitor for Caspase-11, has been shown to suppress LPS-induced inflammatory response in macrophage cell line;[44] however, it failed to preserve NAD+ concentrations, suggesting that MCM-induced neurotoxicity is not mediated via these caspases (Figs. 7B,C and S5). Furthermore, Necrostatin-1 (Nec-1), a RIPK1 inhibitor,[38] and GSK872' targeting RIPK3,[45] did

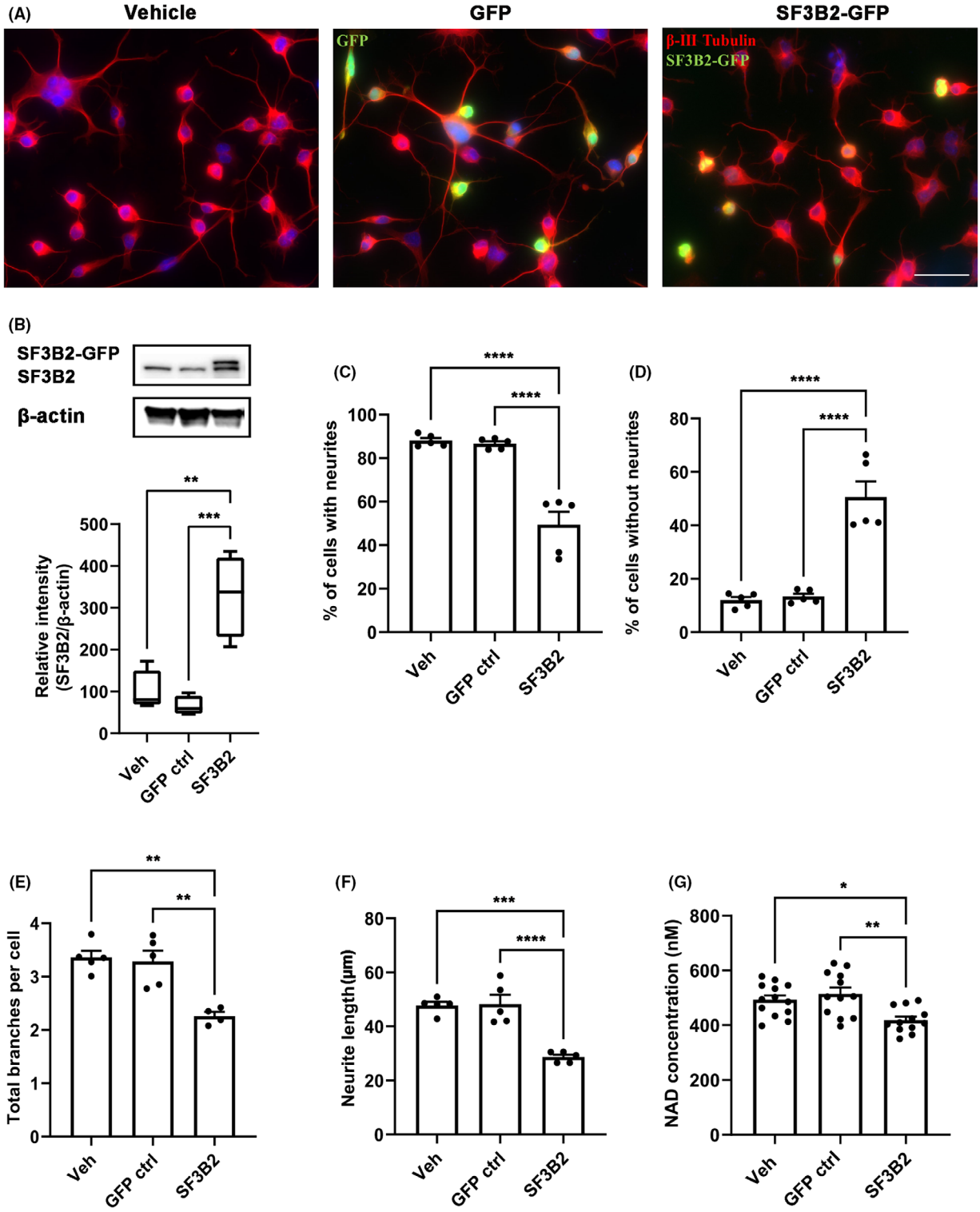

Figure 4. Overexpression of SF3B2 impairs neurite development and integrity. (A) Representative images of differentiated N2A cells treated with vehicle or transfected with 0.5 μg of GFP control or SF3B2-GFP plasmid (bar = 50 μm). (B) Representative image and quantitation of SF3B2 overexpression. (C) Percentage of cells having neurites. (D) Percentage of cells without neurites. (E) Quantification of total branches per cell. (F) Quantification of neurite length. (G) Measurement of NAD+ concentration in differentiated N2A cells. All data are shown as mean ± SEM with $n = 4$–5 from each independent experiments. *$p < 0.05$, **$p < 0.01$, ***$p < 0.001$, ****$p < 0.0001$.

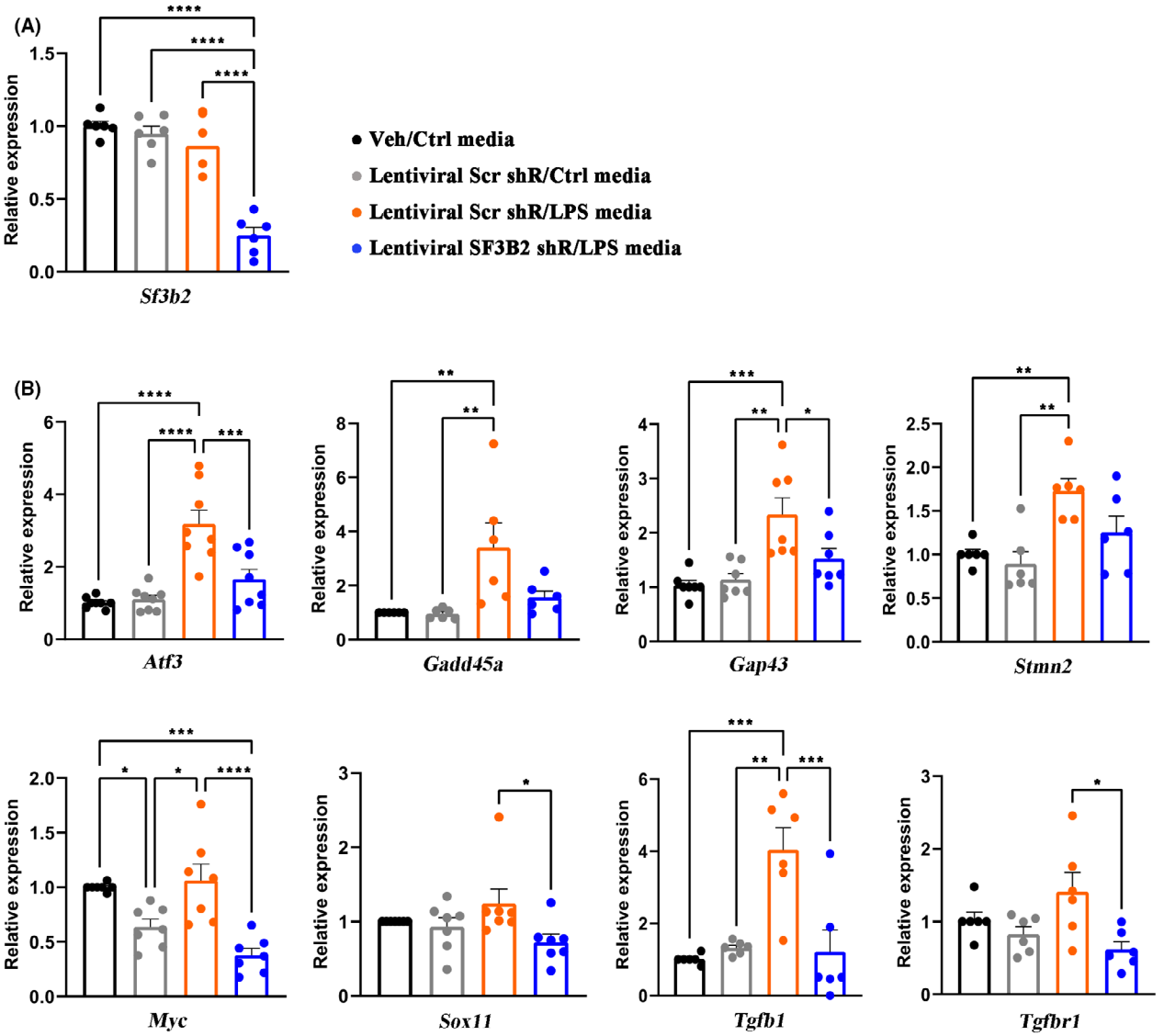

Figure 5. Lentiviral-mediated knockdown of SF3B2 in cortical neurons reduces the transcription of regeneration-associated genes (RAG) after exposure to inflammatory insult. Cortical neurons were exposed to MCM for 24 h at DIV9 following lentiviral transduction at DIV6. mRNA expression levels of *Sf3b2* (A) and regeneration-associated genes (RAG) (B). The combination of three reference genes, *18SR1*, *Hprt*, and *Hmbs*, was used as a loading control. All data are shown as mean ± SEM with at least five independent experiments. *$p < 0.05$, **$p < 0.01$, ***$p < 0.001$, ****$p < 0.0001$.

not prevent NAD+ loss caused by MCM (Fig. S5). Collectively, these results indicate that both apoptosis and necroptosis are not the direct mechanisms targeted by reduced SF3B2 to prevent inflammatory axonal injury.

Discussion

In this study, we show that reduction of SF3B2 protein level in CNS neurons by RNAi is sufficient to prevent RGC loss and axon degeneration and preserve myelin integrity in EAE and protects neuronal viability and axonal integrity against inflammatory injury. We further show that SF3B2 downregulation suppresses the transcription of RAG and necroptosis genes which are markedly upregulated following exposure to MCM. Together, our findings suggest that targeting SF3B2 could be a promising strategy to protect CNS neurons and their axonal integrity from inflammatory neurodegeneration.

Current MS therapies primarily focus on modulating autoimmune response, which can effectively alleviate inflammation and slow down the disease progression at early stages.[3,4] However, there are currently limited

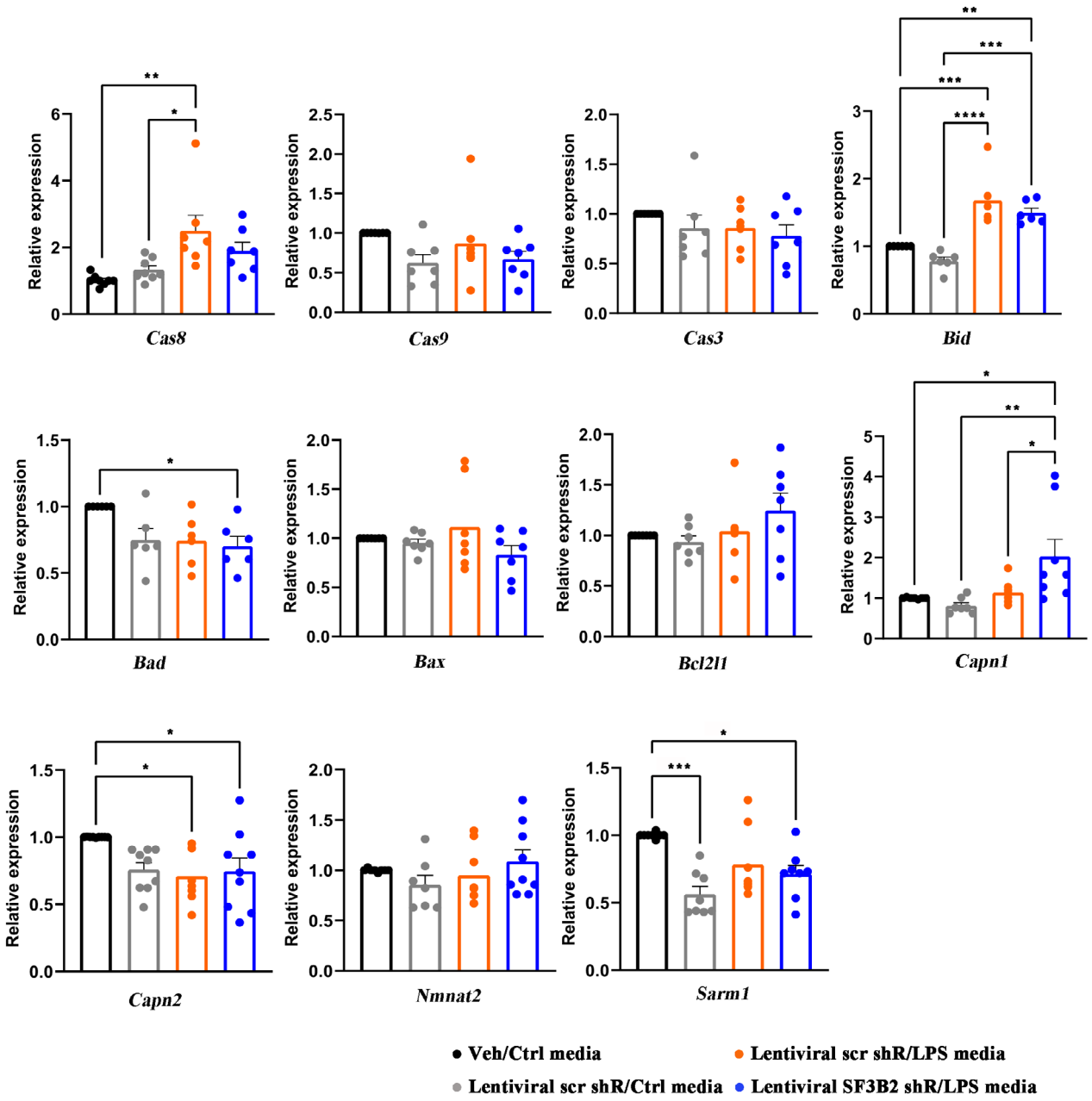

Figure 6. Expression of genes involved in apoptosis pathways are not significantly modulated by MCM or SF3B2 knockdown. Cortical neurons were exposed to MCM for 24 h following lentiviral transduction and mRNA expression levels of apoptosis-related genes were measured. The combination of three reference genes, *18SR1*, *Hprt*, and *Hmbs*, was used as a loading control. All data are shown as mean ± SEM of five independent experiments. *$p < 0.05$, **$p < 0.01$, ***$p < 0.001$, ****$p < 0.0001$.

therapies directed at the secondary axonal loss and neurodegeneration. Thus, many researchers have been trying to find potential therapeutics that promote remyelination and directly protect neurons from degeneration. It has been shown that treatment with ursolic acid in EAE mice at the chronic phase was able to not only mitigate clinical symptoms but also reduce axon degeneration and promote remyelination through oligodendrocyte maturation.[46] Another group showed that SRT 501, a pharmaceutical formulation of resveratrol and an activator of SIRT1, prevented RGC loss and delayed visual dysfunction in chronic EAE without alleviating CNS inflammation.[47] Neuroprotection induced by directly altering the expression of target genes has been explored as well.

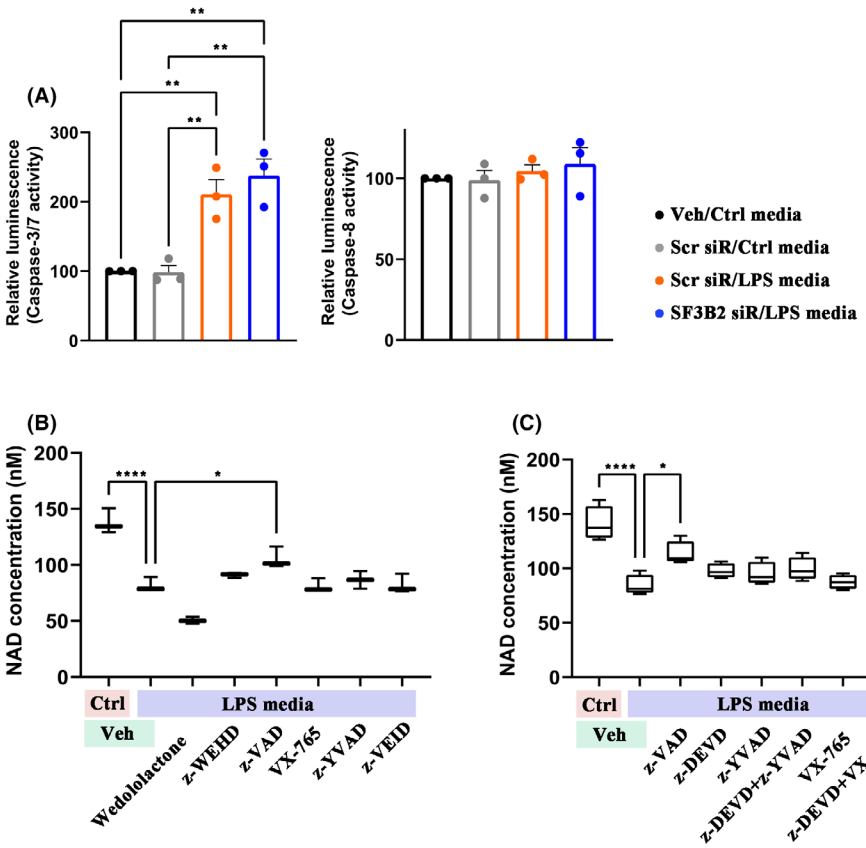

Figure 7. Apoptosis is neither the target modulated by SF3B2 knockdown-induced neuroprotection nor the key mechanism mediating MCM-induced axonal injury. Differentiated N2A cells (A–C) were exposed to MCM for 24 h following siRNA transfection (A) or the incubation with caspase inhibitors (B, C). (A) Measurement of caspase-3/7 and -8 activity in differentiated N2A cells. (B, C) Measurement of NAD+ concentrations in differentiated N2A cells. A pan-caspase inhibitor z-VAD-FMK (50 μM), z-DEVD-FMK (25 μM) targeting Caspase-3, -6, -7, -8, and -10, Wedelolactone (10 μM) inhibiting Caspase-11, z-WEHD-FMK (20 μM) suppressing Caspase-1,-8,-11, VX-765 (20 μM) inhibiting Caspase-1 and -4, z-YVAD-FMK (20 μM) targeting Caspase-1, -11, and z-VEID-FMK suppressing Caspase-6 were used as negative modulators for caspase activity. All data are shown as mean ± SEM of three to four independent experiments *$p < 0.05$, **$p < 0.01$, ****$p < 0.0001$.

Neuron-specific overexpression of SIRT1 in EAE mice suppressed neuronal apoptosis in the injured spinal cords and attenuated clinical symptoms and diminished the level of demyelination and axon injury in the spinal cord.[48] Similarly, fingolimod and other sphingosine 1-phosphate receptor agonists have been shown to have neuroprotective effects in mouse models of MS.[49,50] However, none of these strategies have resulted in clinical success yet.

Our previous studies found that ethoxyquin (EQ) and its novel analog, EQ-6 (6-(5-amino)-ethoxy-2,2,4-trimethyl-1,2-dihydroquinoline hydrochloride), prevent axonal degeneration induced in rat dorsal root ganglion (DRG) neurons treated with cisplatin or paclitaxel and mouse models of chemotherapy-induced peripheral neuropathy (CIPN).[7,51,52] EQ is an FDA-approved food preservative, and it is added in animal feed.[51] Through subsequent experiments, we showed that EQ interacts with heat shock protein 90 (Hsp90) and negatively modulates its chaperone function, resulting in diminished cellular level of SF3B2 protein.[7,52] Interestingly, direct knockdown of SF3B2 by RNAi was sufficient to make rat DRG neuronal cells resistant to cisplatin-induced toxicity.[7] In the current study we observed that this strategy is also effective to preserve CNS neurons from inflammatory neurotoxicity in experimental models for MS. It remains unclear whether EQ or EQ-6 can provide CNS protection following inflammatory injury. If EQ-6 is identified to exert neuroprotective effects in animal models of CNS diseases as well, it might be worth developing and utilizing EQ-6 as a promising pharmacological approach to prevent neurodegeneration, given that EQ-6 is likely to accumulate in neural tissue and lacks significant genotoxicity and carcinogenicity.[51] Other strategies that can also

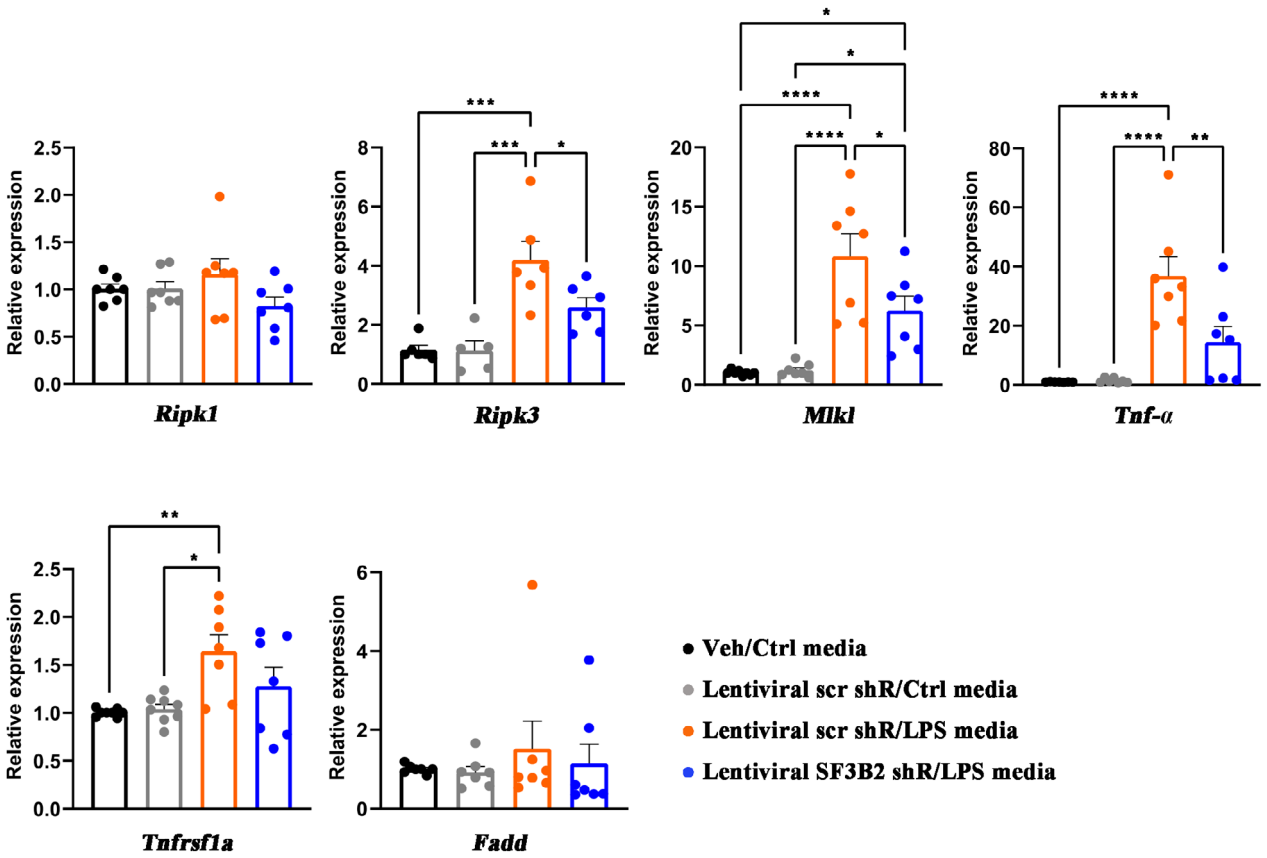

Figure 8. Lentiviral-mediated knockdown of SF3B2 suppresses the transcription of necroptosis genes in cortical neurons after MCM treatment. Cortical neurons were exposed to MCM for 24 h following lentiviral transduction, and then mRNA expression levels of necroptosis-related genes were measured. The combination of three reference genes, *18SR1*, *Hprt*, *Hmbs*, was used as a loading control. All data are shown as mean ± SEM of five independent experiments. *$p < 0.05$, **$p < 0.01$, ***$p < 0.001$, ****$p < 0.0001$.

reduce SF3B2 levels include anti-sense oligos, which have been shown to be effective in several neurodegenerative studies including spinal muscular atrophy and amyloid neuropathy.[53,54]

A major challenge in developing therapies for CNS axonal protection is targeting the appropriate cell types while reducing complications due to off-target side effects. We were able to achieve this by exploiting the tropism of AAV2/PHP.eb particles toward CNS neurons[10,11] and delivering it directly into the eye. We were able to lower the cellular level of SF3B2 in RGC neurons in a stable manner throughout the duration of the in vivo experiments. This was sufficient to improve RGC survival, axonal integrity, and myelin defects in EAE mice. Obviously, this approach is a preventative measure as we had to deliver the AAV-shRNA well in advance of inducing the EAE, and accordingly, it may not be a feasible clinical approach in MS patients. Nevertheless, patients with optic neuritis do suffer from secondary axonal degeneration and this is often delayed compared to the initial inflammatory demyelination.[55,56] The time between the onset of optic neuritis and development of delayed axonal degeneration may offer a therapeutic window to target the SF3B2 in RGC neurons and reduce the likelihood of long-term decreased vision.

Although the in vivo EAE model does not render itself to detailed mechanistic molecular studies, the axonal degeneration seen in inflammatory insults can be modeled in vitro. In this study, we treated cortical neurons with the supernatant of LPS-stimulated microglia cell line. Microglia are the resident immune cells in the CNS and play a key role in the pathogenesis of MS.[57–59] In response to the treatment with LPS, they have been shown to produce excess amount of TNF-α, IFN-γ, and IL-6, which are the main soluble mediators of immune response in active MS lesions.[16–18] TNF-α from activated microglia is known to inhibit cell survival signaling and induce caspase-dependent apoptosis, resulting in neurodegeneration.[60,61] Apoptosis by Fas ligand which is secreted from stimulated microglia potentiates TNF-α-mediated

neurotoxicity.[62] Neurite beading and swellings, and neuronal death are also caused by IFN-γ treatment.[60] The extent of neurotoxicity by one inflammatory factor itself is weak, however, conditioned media from microglia stimulated with LPS contain diverse neurotoxic cytokines and free radicals which induce marked neuronal injury.[60]

Like these previous studies, we found that conditioned media from LPS-stimulated microglia cell line is able to cause neuronal and axonal damage. In addition to demonstrating axonal degeneration, we also confirmed that MCM likely activated SARM1 (Figs. 3F and 7B,C, S4E and S5), a key mediator of Wallerian degeneration.[63] When SARM1 is activated, the TIR (Toll/Interleukin-1 Receptor) domain dimerizes and exposes a NAD hydrolase activity, which results in reduced cellular levels of NAD.[64] In our cultures, we found that MCM-treated cultures had reduced NAD levels and that this reduction in NAD+ was prevented in neuronal cultures where SF3B2 protein expression was reduced by about 50%.

How the reduced level of SF3B2 prevents activation of SARM1 is unclear. We examined the mRNA levels of NMNAT1 and SARM1 but did not see any significant differences in cultures treated with MCM or SF3B2 RNAi. Although SF3B2 is an RNA binding protein,[65] it is likely that neuroprotection seen with reduced levels of SF3B2 is not mediated through altered transcription of NMNAT2 and SARM1, two key molecules involved in Wallerian degeneration.[63]

Given these negative findings, we explored the changes in other enzymatic pathways implicated in MCM-induced neurotoxicity. We did not observe any meaningful significant changes in gene expression or enzymatic activity of classical apoptosis pathway, but expression levels of several genes involved in necroptosis were upregulated in MCM-treated neurons, specifically, *Tnf-α*, *Ripk3*, *and Mlkl*. TNF-α signaling with other inflammatory factors released by activated microglia triggers RIPK1-RIPK3-MLKL axis required for necroptosis.[30,66] In addition, neurons have been shown to express TNF-α following injury,[67] suggesting that TNF-α-induced necroptotic mechanism is a potential key pathway in neurotoxicity of conditioned media from LPS-stimulated microglia. However, we did not see any significant change in the activation of Caspase-8, a mediator of canonical necroptosis pathway,[68] and we were unable to block NAD+ loss with necroptosis inhibitors, indicating that axonal degeneration may not be wholly mediated via the TNF-α-induced RIPK1-RIPK3-MLKL axis. Nevertheless, the MCM-induced upregulation of *Tnf-α*, *Ripk3*, and *Mlkl* was prevented in neurons where SF3B2 level was downregulated. This suggests that SF3B2-mediated neuroprotection may be multipronged, acting at several key pathways. TNF-α causes a rise in intracellular calcium concentration,[69] which plays a role in injury response.[70] It is possible that SF3B2 knockdown inhibited a rise in calcium and thereby prevented the upregulation of RAG genes.

An interesting observation we made was the consistent inhibition of MCM-induced axon degeneration, as assessed by NAD+ levels, with pan-caspase inhibitor z-VAD-FMK.[39] However, we were unable to replicate similar inhibition with more specific inhibitors, such as z-DEVD-FMK targeting Caspase-3, -7, -8, and -10,[40] Wedelolactone blocking Caspase-11,[44] or Nect-1 targeting RIPK1,[45] suggesting that the effect of z-VAD-FMK may not be via the canonical caspase or necroptosis pathways. It is possible that z-VAD-FMK inhibited calpains[71,72] which are one of the most downstream mediators of Wallerian axon degeneration,[73] but the fact that z-VAD-FMK was able to prevent NAD+ loss suggests that the effect is upstream of SARM1. Future studies are needed to further dissect the molecular mechanisms of MCM-induced neurotoxicity and axon degeneration and how this is prevented by downregulating SF3B2 levels.

Nevertheless, our findings consistently show that downregulation of SF3B2 is sufficient to prevent neurotoxicity and secondary axonal degeneration induced by inflammatory signaling in vitro and in vivo. This suggests that further examination of strategies to regulate SF3B2 levels as a viable therapeutic target for optic neuritis and MS patients is warranted.

Acknowledgments

The authors are thankful to Lee J. Martin, Peter Calabresi, and Donald J. Zack for discussion and valuable inputs for our study. We thank Michele Pucak at Multiphoton Imaging Core (Johns Hopkins University) and Carol Cooke at Neuromuscular Pathology Laboratory (Johns Hopkins University) for their technical advice and assistance on imaging and data analysis. We also thank Chen Wang, Yiming Zhang, and Zhigang He at the Boston Children's Hospital Viral Core for technical assistance in virus work. This work was supported by grants from Race to Erase MS Foundation and Dr. Miriam and Sheldon G. Adelson Medical Foundation and a generous donation from the Merkin Family Foundation.

Author contributions

A.H. and Y.J. conceived and designed the experiments and wrote the manuscript. Y.J. performed experiments and collected and analyzed data with input from A.H. A.H. supervised the work and acquired funding. B.K. assisted in data analysis and animal experiments. L.R. and A.V. provided microfluidic devices and helped in the preparation of devices for cultures. All authors approved the final manuscript.

Conflict of interests

Under a license agreement between AxoProtego Therapeutics LLC and the Johns Hopkins University, Dr. Hoke and the University are entitled to royalty distributions related to the technology discussed in this publication related to ethoxyquin derivatives. Dr. Hoke also is a founder and serves as the Chair of AxoProtego Therapeutics LLC's, Scientific Advisory Board. This arrangement has been reviewed and approved by the Johns Hopkins University in accordance with its conflict-of-interest policies.

References

1. Filippi M, Bar-Or A, Piehl F, et al. Multiple sclerosis. Nat Rev Dis Primers. 2018;4:43. doi:10.1038/s41572-018-0041-4
2. Greer JM, McCombe PA. Role of gender in multiple sclerosis: clinical effects and potential molecular mechanisms. J Neuroimmunol. 2011;234:7-18. doi:10.1016/j.jneuroim.2011.03.003
3. Baecher-Allan C, Kaskow BJ, Weiner HL. Multiple sclerosis: mechanisms and immunotherapy. Neuron. 2018;97:742-768. doi:10.1016/j.neuron.2018.01.021
4. Farooqi N, Gran B, Constantinescu CS. Are current disease-modifying therapeutics in multiple sclerosis justified on the basis of studies in experimental autoimmune encephalomyelitis? J Neurochem. 2010;115:829-844. doi:10.1111/j.1471-4159.2010.06982.x
5. Golas MM, Sander B, Will CL, Luhrmann R, Stark H. Molecular architecture of the multiprotein splicing factor SF3b. Science. 2003;300:980-984. doi:10.1126/science.1084155
6. Will CL, Urlaub H, Achsel T, Gentzel M, Wilm M, Lührmann R. Characterization of novel SF3b and 17 S U2 snRNP proteins, including a human Prp5p homologue and an SF3b DEAD-box protein. EMBO J. 2002;21:4978-4988. doi:10.1093/emboj/cdf480
7. Zhu J, Carozzi VA, Reed N, et al. Ethoxyquin provides neuroprotection against cisplatin-induced neurotoxicity. Sci Rep. 2016;6:28861. doi:10.1038/srep28861
8. Jin J, Smith MD, Kersbergen CJ, et al. Glial pathology and retinal neurotoxicity in the anterior visual pathway in experimental autoimmune encephalomyelitis. Acta Neuropathol Commun. 2019;7:125. doi:10.1186/s40478-019-0767-6
9. Aktas O, Ullrich O, Infante-Duarte C, Nitsch R, Zipp F. Neuronal damage in brain inflammation. Arch Neurol. 2007;64:185-189. doi:10.1001/archneur.64.2.185
10. Mathiesen SN, Lock JL, Schoderboeck L, Abraham WC, Hughes SM. CNS transduction benefits of AAV-PHP.eB over AAV9 are dependent on administration route and mouse strain. Mol Ther Methods Clin Dev. 2020;19:447-458. doi:10.1016/j.omtm.2020.10.011
11. Chan KY, Jang MJ, Yoo BB, et al. Engineered AAVs for efficient noninvasive gene delivery to the central and peripheral nervous systems. Nat Neurosci. 2017;20:1172-1179. doi:10.1038/nn.4593
12. Masin L, Claes M, Bergmans S, et al. A novel retinal ganglion cell quantification tool based on deep learning. Sci Rep. 2021;11:702. doi:10.1038/s41598-020-80308-y
13. Narciso MS, Hokoc JN, Martinez AM. Watery and dark axons in Wallerian degeneration of the opossum's optic nerve: different patterns of cytoskeletal breakdown? An Acad Bras Cienc. 2001;73:231-243. doi:10.1590/s0001-37652001000200008
14. Park JW, Kim HJ, Kang MW, Jeon NL. Advances in microfluidics-based experimental methods for neuroscience research. Lab Chip. 2013;13:509-521. doi:10.1039/c2lc41081h
15. Maldonado RF, Sá-Correia I, Valvano MA. Lipopolysaccharide modification in gram-negative bacteria during chronic infection. FEMS Microbiol Rev. 2016;40:480-493. doi:10.1093/femsre/fuw007
16. Benveniste EN. Role of macrophages/microglia in multiple sclerosis and experimental allergic encephalomyelitis. J Mol Med. 1997;75:165-173. doi:10.1007/s001090050101
17. Lee SC, Liu W, Dickson DW, Brosnan CF, Berman JW. Cytokine production by human fetal microglia and astrocytes. Differential induction by lipopolysaccharide and IL-1 beta. J Immunol. 1993;150:2659-2667.
18. Olson JK, Miller SD. Microglia initiate central nervous system innate and adaptive immune responses through multiple TLRs. J Immunol. 2004;173:3916-3924. doi:10.4049/jimmunol.173.6.3916
19. Blank M, Enzlein T, Hopf C. LPS-induced lipid alterations in microglia revealed by MALDI mass spectrometry-based cell fingerprinting in neuroinflammation studies. Sci Rep. 2022;12:2908. doi:10.1038/s41598-022-06894-1
20. Kwon J, Arsenis C, Suessmilch M, McColl A, Cavanagh J, Morris BJ. Differential effects of toll-like receptor activation and differential mediation by MAP kinases of immune responses in microglial cells. Cell Mol Neurobiol. 2022;42:2655-2671. doi:10.1007/s10571-021-01127-x
21. Paglini G, Peris L, Mascotti F, Quiroga S, Caceres A. Tau protein function in axonal formation. Neurochem Res. 2000;25:37-42. doi:10.1023/a:1007531230651
22. Erecińska M, Silver IA. ATP and brain function. J Cereb Blood Flow Metab. 1989;9:2-19. doi:10.1038/jcbfm.1989.2
23. Coleman MP, Höke A. Programmed axon degeneration: from mouse to mechanism to medicine. Nat Rev Neurosci. 2020;21:183-196. doi:10.1038/s41583-020-0269-3
24. Wang J, He Z. NAD and axon degeneration: from the Wlds gene to neurochemistry. Cell Adh Migr. 2009;3:77-87. doi:10.4161/cam.3.1.7483
25. Ma TC, Willis DE. What makes a RAG regeneration associated? Front Mol Neurosci. 2015;8:43. doi:10.3389/fnmol.2015.00043

26. Moore DL, Goldberg JL. Multiple transcription factor families regulate axon growth and regeneration. Dev Neurobiol. 2011;71:1186-1211. doi:10.1002/dneu.20934
27. Qian C, Zhou F-Q. Updates and challenges of axon regeneration in the mammalian central nervous system. J Mol Cell Biol. 2020;12:798-806. doi:10.1093/jmcb/mjaa026
28. Tsujino H, Kondo E, Fukuoka T, et al. Activating transcription factor 3 (ATF3) induction by axotomy in sensory and motoneurons: a novel neuronal marker of nerve injury. Mol Cell Neurosci. 2000;15:170-182. doi:10.1006/mcne.1999.0814
29. Li S, Gu X, Yi S. The regulatory effects of transforming growth factor-beta on nerve regeneration. Cell Transplant. 2017;26:381-394. doi:10.3727/096368916X693824
30. Dhuriya YK, Sharma D. Necroptosis: a regulated inflammatory mode of cell death. J Neuroinflammation. 2018;15:199. doi:10.1186/s12974-018-1235-0
31. Moujalled D, Strasser A, Liddell JR. Molecular mechanisms of cell death in neurological diseases. Cell Death Differ. 2021;28:2029-2044. doi:10.1038/s41418-021-00814-y
32. Noailles A, Maneu V, Campello L, Lax P, Cuenca N. Systemic inflammation induced by lipopolysaccharide aggravates inherited retinal dystrophy. Cell Death Dis. 2018;9:350. doi:10.1038/s41419-018-0355-x
33. McIlwain DR, Berger T, Mak TW. Caspase functions in cell death and disease. Cold Spring Harb Perspect Biol. 2013;5:a008656. doi:10.1101/cshperspect.a008656
34. Li J, Yuan J. Caspases in apoptosis and beyond. Oncogene. 2008;27:6194-6206. doi:10.1038/onc.2008.297
35. Picon C, Jayaraman A, James R, et al. Neuron-specific activation of necroptosis signaling in multiple sclerosis cortical grey matter. Acta Neuropathol. 2021;141:585-604. doi:10.1007/s00401-021-02274-7
36. Andersson M, Sjostrand J, Petersen A, Honarvar AK, Karlsson JO. Caspase and proteasome activity during staurosporin-induced apoptosis in lens epithelial cells. Invest Ophthalmol Vis Sci. 2000;41:2623-2632.
37. Okun I, Malarchuk S, Dubrovskaya E, et al. Screening for caspase-3 inhibitors: a new class of potent small-molecule inhibitors of caspase-3. J Biomol Screen. 2006;11:277-285. doi:10.1177/1087057105285048
38. Cao L, Mu W. Necrostatin-1 and necroptosis inhibition: pathophysiology and therapeutic implications. Pharmacol Res. 2021;163:105297. doi:10.1016/j.phrs.2020.105297
39. Dhani S, Zhao Y, Zhivotovsky B. A long way to go: caspase inhibitors in clinical use. Cell Death Dis. 2021;12:949. doi:10.1038/s41419-021-04240-3
40. Yoshimori A, Sakai J, Sunaga S, et al. Structural and functional definition of the specificity of a novel caspase-3 inhibitor, Ac-DNLD-CHO. BMC Pharmacol. 2007;7:8. doi:10.1186/1471-2210-7-8
41. Kim MJ, Yoo JY. Active caspase-1-mediated secretion of retinoic acid inducible gene-I. J Immunol. 2008;181:7324-7331. doi:10.4049/jimmunol.181.10.7324
42. Huang WC, Gu PY, Fang LW, Huang YL, Lin CF, Liou CJ. Sophoraflavanone G from *Sophora flavescens* induces apoptosis in triple-negative breast cancer cells. Phytomedicine. 2019;61:152852. doi:10.1016/j.phymed.2019.152852
43. Mintzer R, Ramaswamy S, Shah K, et al. A whole cell assay to measure caspase-6 activity by detecting cleavage of Lamin a/C. PLoS One. 2012;7:e30376. doi:10.1371/journal.pone.0030376
44. Yuan F, Chen J, Sun PP, Guan S, Xu J. Wedelolactone inhibits LPS-induced pro-inflammation via NF-kappaB pathway in RAW 264.7 cells. J Biomed Sci. 2013;20:84. doi:10.1186/1423-0127-20-84
45. Duan X, Liu X, Liu N, et al. Inhibition of keratinocyte necroptosis mediated by RIPK1/RIPK3/MLKL provides a protective effect against psoriatic inflammation. Cell Death Dis. 2020;11:134. doi:10.1038/s41419-020-2328-0
46. Zhang Y, Li X, Ciric B, et al. A dual effect of ursolic acid to the treatment of multiple sclerosis through both immunomodulation and direct remyelination. Proc Natl Acad Sci U S A. 2020;117:9082-9093. doi:10.1073/pnas.2000208117
47. Shindler KS, Ventura E, Dutt M, Elliott P, Fitzgerald DC, Rostami A. Oral resveratrol reduces neuronal damage in a model of multiple sclerosis. J Neuroophthalmol. 2010;30:328-339. doi:10.1097/WNO.0b013e3181f7f833
48. Nimmagadda VK, Bever CT, Vattikunta NR, et al. Overexpression of SIRT1 protein in neurons protects against experimental autoimmune encephalomyelitis through activation of multiple SIRT1 targets. J Immunol. 2013;190:4595-4607. doi:10.4049/jimmunol.1202584
49. Slowik A, Schmidt T, Beyer C, Amor S, Clarner T, Kipp M. The sphingosine 1-phosphate receptor agonist FTY720 is neuroprotective after cuprizone-induced CNS demyelination. Br J Pharmacol. 2015;172:80-92. doi:10.1111/bph.12938
50. Yang T, Zha Z, Yang X, et al. Neuroprotective effects of fingolimod supplement on the retina and optic nerve in the mouse model of experimental autoimmune encephalomyelitis. Front Neurosci. 2021;15:663541. doi:10.3389/fnins.2021.663541
51. Cetinkaya-Fisgin A, Zhu J, Luan X, et al. Development of EQ-6, a novel analogue of ethoxyquin to prevent chemotherapy-induced peripheral neuropathy. Neurotherapeutics. 2021;18:2061-2072. doi:10.1007/s13311-021-01093-8
52. Zhu J, Chen W, Mi R, Zhou C, Reed N, Höke A. Ethoxyquin prevents chemotherapy-induced neurotoxicity via Hsp90 modulation. Ann Neurol. 2013;74:893-904. doi:10.1002/ana.24004
53. Ackermann EJ, Guo S, Booten S, et al. Clinical development of an antisense therapy for the treatment of transthyretin-associated polyneuropathy. Amyloid. 2012;19 (Suppl 1):43-44. doi:10.3109/13506129.2012.673140

54. Mercuri E, Darras BT, Chiriboga CA, et al. Nusinersen versus sham control in later-onset spinal muscular atrophy. N Engl J Med. 2018;378:625-635. doi:10.1056/NEJMoa1710504
55. You Y, Barnett MH, Yiannikas C, et al. Chronic demyelination exacerbates neuroaxonal loss in patients with MS with unilateral optic neuritis. Neurol Neuroimmunol Neuroinflamm. 2020;7:e700. doi:10.1212/NXI.0000000000000700
56. Stadelmann C, Wegner C, Bruck W. Inflammation, demyelination, and degeneration—recent insights from MS pathology. Biochim Biophys Acta. 2011;1812:275-282. doi:10.1016/j.bbadis.2010.07.007
57. Guerrero BL, Sicotte NL. Microglia in multiple sclerosis: friend or foe? Front Immunol. 2020;11:374. doi:10.3389/fimmu.2020.00374
58. Luo C, Jian C, Liao Y, et al. The role of microglia in multiple sclerosis. Neuropsychiatr Dis Treat. 2017;13:1661-1667. doi:10.2147/NDT.S140634
59. Voet S, Prinz M, van Loo G. Microglia in central nervous system inflammation and multiple sclerosis pathology. Trends Mol Med. 2019;25:112-123. doi:10.1016/j.molmed.2018.11.005
60. Takeuchi H, Jin S, Wang J, et al. Tumor necrosis factor-α induces neurotoxicity via glutamate release from hemichannels of activated microglia in an autocrine manner*. J Biol Chem. 2006;281:21362-21368. doi:10.1074/jbc.M600504200
61. Block ML, Hong JS. Microglia and inflammation-mediated neurodegeneration: multiple triggers with a common mechanism. Prog Neurobiol. 2005;76:77-98. doi:10.1016/j.pneurobio.2005.06.004
62. Taylor DL, Jones F, Kubota ES, Pocock JM. Stimulation of microglial metabotropic glutamate receptor mGlu2 triggers tumor necrosis factor alpha-induced neurotoxicity in concert with microglial-derived Fas ligand. J Neurosci. 2005;25:2952-2964. doi:10.1523/JNEUROSCI.4456-04.2005
63. Gerdts J, Summers DW, Milbrandt J, DiAntonio A. Axon self-destruction: new links among SARM1, MAPKs, and NAD+ metabolism. Neuron. 2016;89:449-460. doi:10.1016/j.neuron.2015.12.023
64. Essuman K, Summers DW, Sasaki Y, Mao X, DiAntonio A, Milbrandt J. The SARM1 toll/Interleukin-1 receptor domain possesses intrinsic NAD(+) cleavage activity that promotes pathological axonal degeneration. Neuron. 2017;93:1334-1343 e1335. doi:10.1016/j.neuron.2017.02.022
65. Kawamura N, Nimura K, Saga K, et al. SF3B2-mediated RNA splicing drives human prostate cancer progression. Cancer Res. 2019;79:5204-5217. doi:10.1158/0008-5472.CAN-18-3965
66. Yuan J, Amin P, Ofengeim D. Necroptosis and RIPK1-mediated neuroinflammation in CNS diseases. Nat Rev Neurosci. 2019;20:19-33. doi:10.1038/s41583-018-0093-1
67. Probert L. TNF and its receptors in the CNS: the essential, the desirable and the deleterious effects. Neuroscience. 2015;302:2-22. doi:10.1016/j.neuroscience.2015.06.038
68. Bertheloot D, Latz E, Franklin BS. Necroptosis, pyroptosis and apoptosis: an intricate game of cell death. Cell Mol Immunol. 2021;18:1106-1121. doi:10.1038/s41423-020-00630-3
69. Koller H, Thiem K, Siebler M. Tumour necrosis factor-alpha increases intracellular Ca2+ and induces a depolarization in cultured astroglial cells. Brain. 1996;119 (Pt 6):2021-2027. doi:10.1093/brain/119.6.2021
70. Marambaud P, Dreses-Werringloer U, Vingtdeux V. Calcium signaling in neurodegeneration. Mol Neurodegener. 2009;4:20. doi:10.1186/1750-1326-4-20
71. Bang B, Baadsgaard O, Skov L, Jaattela M. Inhibitors of cysteine cathepsin and calpain do not prevent ultraviolet-B-induced apoptosis in human keratinocytes and HeLa cells. Arch Dermatol Res. 2004;296:67-73. doi:10.1007/s00403-004-0473-4
72. Nakajima E, Hammond KB, Shearer TR, Azuma M. Activation of the mitochondrial caspase pathway and subsequent calpain activation in monkey RPE cells cultured under zinc depletion. Eye (Lond). 2014;28:85-92. doi:10.1038/eye.2013.239
73. Yang J, Wu Z, Renier N, et al. Pathological axonal death through a MAPK cascade that triggers a local energy deficit. Cell. 2015;160:161-176. doi:10.1016/j.cell.2014.11.053

Supporting Information

Additional supporting information may be found online in the Supporting Information section at the end of the article.

Figure S1. Whole mount retinal immunohistochemistry showing AAV transduction in RGCs and knockdown efficiency of AAV-Sf3b2 shRNA in vitro and in vivo. (A) Representative images of whole-mount retinas transduced with AAV. (B) Confocal images of flat-mounted retina showing GFP, anti-Brn3A, and a merged image. (C and D) Fluorescence intensity of SF3B2 in RGCs at 2 weeks (C) and 8 weeks (D) post-virus administration into the vitreous body. Total fluorescence intensity in cells was divided by respective cellular volume by Imaris, and retinas infected with AAV-GFP were used as a control (n = 6). (E) Sf3b2 mRNA levels from N2A cells were transduced with AAV for 5 days. The combination of three reference genes, 18SR1, Hprt, and Hmbs, was used as a loading control (n = 3). All data are shown as mean ± SEM and n = total number of biological replicates. *$p < 0.0001$.

Figure S2. Validation of AAV safety in RGCs. (A,B) Quantification of RGC survival at 2 weeks (A) and 8 weeks (B) post-intravitreal delivery of AAV ($n \geq 5$ for (A), $n \geq 6$ for (B)). (C and D) Quantification of healthy myelinated axons at 2 weeks (C) and 8 weeks (D) post-intravitreal delivery of AAV ($n \geq 5$ for (C), $n \geq 6$ for

(D)). All data shown as mean ± SEM and n = total number of biological replicates. *$p < 0.05$, **$p < 0.01$, ***$p < 0.001$, ****$p < 0.0001$.

Figure S3. SF3B2 primary antibody validation and knock down efficiency and specificity of siRNA. (A and B) Western blot analysis (A) and quantification (B) of SF3B2 protein level in N2A cells after the transfection with siRNA for 48 h. (C–E) Western blot analysis (C) and quantification of SF3B3 (D) and SF3B4 (E) after siRNA transfection. Beta-actin was used as a loading control. All data were shown as mean ± SEM and $n = 3$ biological replicates. *$p < 0.05$, **$p < 0.01$, ***$p < 0.001$, ****$p < 0.0001$.

Figure S4. Neurotoxicity of LPS-stimulated microglial media (MCM) and neuroprotection against MCM toxicity in N2A cells via SF3B2 downregulation. (A–D) Western blot analysis (A) and quantification of SF3B2 (B), Capsse-3 (C), and Cleaved-caspase-3 (D) in cortical neurons challenged with MCM for 48 h ($n = 3$). (E) N2A cells were treated with MCM following siRNA transfection. (E) Cell viability of N2A cells ($n = 5$) and (f) western blot analysis ($n = 3$). Beta-actin was used as a loading control. All data are shown as mean ± SEM and n = total number of biological replicates. *$p < 0.05$, **$p < 0.01$, ***$p < 0.001$, ****$p < 0.0001$.

Figure S5. Necroptosis inhibitors do not prevent MCM-induced decline in NAD+ concentrations. Differentiated N2A cells were exposed to MCM for 24 h following the incubation with necroptosis or apoptosis inhibitors and their combinations, and then NAD+ concentrations in differentiated N2A cells were measured. z-DEVD-FMK (25 μM) targeting Caspase-3,-6,-7,-8,-10, and z-VAD-FMK (50 μM) which is a pan-caspase inhibitor, Necrostatin-1 (50 μM) suppressing RIPK1, and GSK'872 which is known to target RIPK3 were used as negative modulators for necroptosis pathway. All data are shown as mean ± SEM and $n = 4$ biological replicates. *$p < 0.05$, **$p < 0.01$, ***$p < 0.001$, ****$p < 0.0001$.

Table S1. Sequences of primers used in RT-PCR experiments.

